Obtaining microparticles of Cu_2O by means of a pulsed discharge of CH_3CH_2OH-N_2

M. C. González, P.G. Reyes, A.Gómez, H. Martínez and V. H. Castrejon

[a]*TecNM/Tecnológico de Estudios Superiores de Jocotitlán (TESJo), Jocotitlán, Estado de México, México.*

[b]*Laboratorio de Física Avanzada, Facultad de Ciencias, Universidad Autonoma del Estado de México, 50200, México.*

[c]*Laboratorio de Espectroscopía, Instituto de Ciencias Físicas, Universidad Nacional Autonoma de México, Morelos C. P. 62210, México.*

[*]*e-mail:marcos.gonzalez@tesjo.edu.mx*

Received 26 October 2022; accepted 23 August 2023

CH_3CH_2OH-N_2 plasma mixture was used to synthesize cuprous oxide (Cu_2O) micro-particles in a pulsed DC sputtering system, using a ethanol pressure of 1.5 Torr and a current of 400 mA at a frequency of 30 kHz. The plasma mixture was used successfully to obtain the micro-particles of Cu_2O using a copper (Cu) target and a stainless steel substrate. The Cu_2O products are characterized by the scanning electron microscope (SEM), the results show that the morphology of the Cu_2O microparticles have a spherical shape which are randomly distributed on the stainless steel substrate. Raman results show that from the CH_3CH_2OH-N_2 plasma mixture it is possible to obtain one of the Cu oxidation phases which corresponds to Cu_2O due to the fact that within the sample analyzed by means of Raman it is possible to observe only the peaks that correspond to the Cu_2O phase. The analysis by energy dispersive spectroscopy (EDS) serves to determine the stoichiometric balance present in the substrate, from which the presence of the characteristic peaks of stainless steel was confirmed, along with the characteristic peaks of Cu and O which exhibit an atomic ratio of 2:1 respectively. Atomic force microscopy (AFM) was used to again determine the morphology of the microparticles, finding a spherical morphology. In addition, the value of roughness and grain size was determined, finding values of 20 nm and 45 nm respectively. The images 3-D show the presence of peaks and valleys within the substrate and an non-homogeneous distribution of spherical micro-particles on the surface of the stainless steel.

Keywords: Plasma; sputtering; micro-particles; Raman spectroscopy; SEM; AFM; EDS.

DOI: https://doi.org/10.31349/RevMexFis.70.011006

1. Introduction

Copper is considered a transition metal with a face-centred cubic structure and a melting point of 1085^oC. When Cu oxidized, it can form several phases such as tenorite (CuO), cuprous oxide (Cu_2O) , $Cu(OH)_2$, Cu_2O_3 and paramelaconite (Cu_4O_3) [1, 2], with CuO and Cu_2O being particularly the most stable phases which have been widely studied due to their electronic characteristics that they carry. Both oxides are p type non-stoichiometric semiconductors, which have a direct band-gap of 2.0-2.2 eV for Cu_2O and of approximately 1.5 eV for CuO. These properties make these phases have a variety of applications in devices in the form of a thin film, mainly in the manufacture of solar cells [3] and lithium-ion batteries, although their applications not only remain there. They can also be used in manufacturing of chemical sensors [4], photo-catalysts [5], capacitors [6], among others. Copper oxides are an attractive material for these applications due to their non-toxicity, low cost and the easy availability of raw materials. Currently are implemented diverse methods for the synthesis of these oxides mainly for Cu_2O in which have been used methods such as electrodeposition [7], thermal oxidation, synthesis wet chemistry [8], spin coating [9], reduction of cupric salts [10] and the implementation of plasmas to obtain these oxides, mainly the Sputtering method [11], from which a diversity of morphologies can be obtained, such is the case of micro-spheres, octahedral, cube-octahedral, hexapoids, rhombic dodecahedra, laminae and plates [12–19], whether synthesized by physical or chemical methods. Physical deposition methods have gained ground because it is a low-cost method with which good results can be obtained, besides that physical parameters can be controlled (pressure, current, sputtering power, substrate bias voltage and target materials). The most used physical method for the synthesis of Cu_2O is Sputtering, ranging from its simplest configuration (DC) to the most sophisticated configuration, Magnetron Sputtering RF. Plasma deposition or activation can also be used for the grafting of different groups of surfaces, as is the case of COOH and OH through a source containing Hydrogen and Oxygen (air, hydrocarbons, etc.) [20–23], mixing it with a plasma containing Nitrogen: N_2, NH_3, N_2/H_2 [24,25]. This work reports the results obtained in a CH_3CH_2OH-N_2 plasma mixture generated from a pulsed discharge using the simplest Sputtering configuration at a pressure of 1.5 Torr and a current of 400 mA at a frequency of 30 kHz, using a Cu target and a stainless steel substrate (alloy iron, zinc and lead) separated at a distance of 40 mm for 60 minutes. The concentrations used to generate

the mixture were 80% CH_3CH_2OH and 20% N_2. The products obtained were analysed by Raman spectroscopy. The morphology was analysed by SEM and AFM. In addition the concentration of each element was analysed by EDS, from which can conclude the obtaining of the microparticles in spherical form of Cu_2O.

2. Experimental setup

Cu_2O microparticles were deposited via a pulsed DC sputtering system (Fig. 1) consisting of a cylindrical stainless-steel chamber 33 cm long, 20 cm in radius, and with a volume of 1.04×10^3 cm^3. As in all Physical Vapour Deposition (PVD) techniques, the base vacuum is very critical, which is why the equipment consists of a vacuum system formed by a rotary vane mechanical pump that reaches a pressure on the order of 1.0×10^{-3} Torr. The system consists of 2 mobile electrodes in which the target and the substrate are placed, the target is made of Cu (High-purity 99.9%) with a diameter of 5 cm and 3 mm in thickness and the stainless steel (Zn, Fe, Cr, S) substrate with a diameter of 6 cm, placed in the center of the vacuum chamber with a separation space of 4.0 cm. These are connected to two electric feedthroughs, which are connected to a power supply, consisted of Pinnacle Plus+ generators, which delivered DC power in a pulsing configuration to enable reactive sputtering. The gas flow within the system is regulated by a flow meter (Matheson Tri. GasFM-1050), which also helps us to control the concentrations of gases within the system, with a proportion of 80% CH_3CH_2OH and 20% N_2 at a constant flux of 1.25 LPM.

To generate plasma, the vacuum chamber is evacuated with a mechanical pump until achieving a base pressure of 2×10^{-1} Torr; next, it is filled with gases (CH_3CH_2OH-N_2), and finally, the discharge was generated by applying a pulsed current of 400 mA at 550 V, with a power of 120 W between two electrodes. Figure 2 shows the voltage (550 V) and current (400 mA) signal applied within the discharge. The black line represents the behaviour of the voltage and the red line corresponds to the current applied during the discharge.

CH_3CH_2OH is used with the intention of giving an application to its reformation and thus being able to take advantage of the species present within the plasma, such is the case of the O atoms, which are the cause of forming one of the

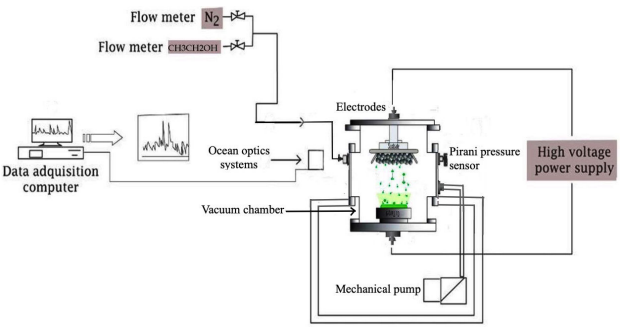

FIGURE 1. Experimental setup.

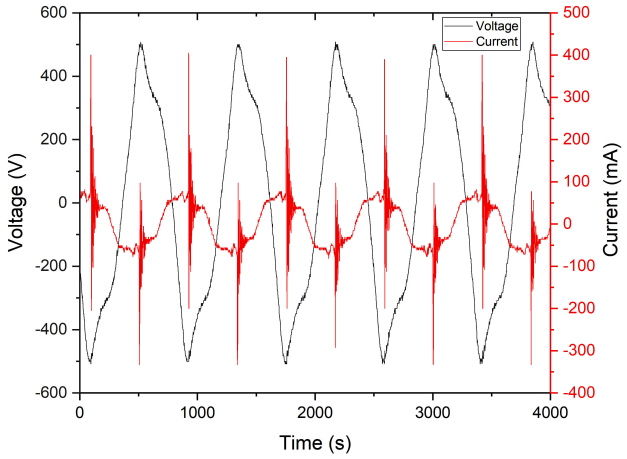

FIGURE 2. Voltage and current output waveforms.

oxidized phases of Cu, in the case of the implementation of N_2, it is with the intention of being able to stabilize the discharge [20–23]. The plasma mixture generated in the pulsed DC Sputtering reactor forms sheaths around the electrodes which are composed of low electron density, the substrate in the sheath generated by the plasma is bombarded with flow of ions and neutral species from the dissociation of CH_3CH_2OH, which can dissociate and form OH species as demonstrated in Refs. [26, 27]. These OH species can interact with the electrons generated by the sheaths which can break the O-H bonds [28] generated by the dissociation of CH_3CH_2OH and thus take advantage of the O species, which can react with the surface of the substrate and the species of the Cu target which are released by the interaction of the plasma with its surface to form the Cu_2O microparticles on the surface of the stainless steel. The bond structure and micro-structure of the thin films were investigated using Raman spectroscopy (micro-Raman, LabRam HR-800 system). Raman measurements were recorded using a He-Ne laser, which was focused using a 50X lens, during the measurements, 60 recoded data were collected every 60 s. SEM (Jeol IT-100 coupled to a Bruker X-Ray microscope) and AFM (EasyScan 2 Flex AFM) were used to determine the thin-film morphology. The SEM microscope was operated in high voltage mode with an accelerating voltage of 20 kV. EDS is used with the intention of verifying the stoichiometric balance present within the analyzed sample.

3. Results and discussion

In this work, a Cu disk was used as a target for the growth of Cu_2O microparticles on the surface of stainless steel. The discharge generated by DC sputtering pulsed was carried out for 60 minutes, using CH_3CH_2OH with the intention of taking advantage of the OH radicals coming from its dissociation, and thanks to the energy inside the plasma, the bonds present can be broken in the OH radicals and to be able to generate O atoms, which can be used to interact with the

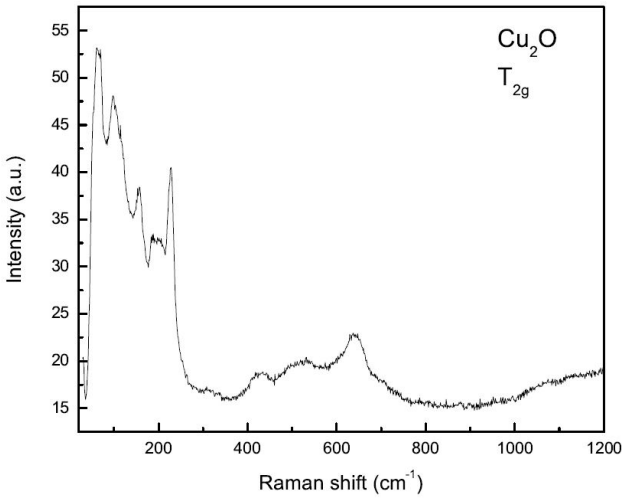

FIGURE 3. Raman spectra microparticles spherical of the Cu_2O.

Cu atoms that are detached from the target with the intention of growing the microparticles on the surface of the stainless steel. Thickness and morphology depend on the gas pressure, sputtering time, voltage and current used to generate the discharge and thus be able to start the atoms from the surface of the Cu which when detached, are carried towards the substrate by medium of the species involved to generate the plasma. SEM studies were carried out on the substrate to observe the formation of adhered Cu_2O structures and thus corroborate the existence of microparticles. The EDS analysis demonstrates the stoichiometry of Cu and O present within the analysed sample. The analysis by Raman spectroscopy demonstrates the structure formed of the Cu_2O microparticles obtained and the AFM analysis corroborate the results obtained by SEM which can be seen to observe its topography, which shows a non-continuous surface on the substrate also showing the morphology of the Cu_2O microparticles.

Figure 3 shows the Raman spectra of the Cu_2O microparticles synthesized using a CH_3CH_2OH-N_2 plasma mixture at a pressure of 1.5 Torr. The spectrum shows different Raman lines at 109, 154, 218, 296, 436, 515, and 638 cm^{-1}.

The mechanism of formation of the microparticles consists of the production of individual atoms from the generated plasma, the subsequent conglomeration of the atoms and the formation of the microparticles, between the steps of formation of atoms and the conglomeration there is an interaction between the atoms coming from N_2 and CH_3CH_2OH species. At this point it is possible the formation of radicals and species that may or may not be stable, such is the case of hydroxyls, oxygen and hydrogen radicals, which are capable of interacting with the atoms coming from the target (Cu) and form one of the Cu oxidized phases. The peak 109 cm^{-1} corresponds to an inactive Raman mode in the sample due to alteration in the crystal system. The peak at 154 cm^{-1} corresponds to an infra-red (IR) Raman mode which is determined by the electron-phonon coupling force, notably depending on the grain size of the microparticles grown on the sample.

TABLE I. Raman Shift and observed peak assignments.

Peak cm^{-1}	**Assignment**
109	Γ_{12}^{-}
154	$\Gamma_{15}^{(1)}(LO)$
218	$2\Gamma_{12}^{-}$
296	$2\Gamma_{15}^{(1)}$
436	$4\Gamma_{12}^{-}$
515	T_{2g}
638	TO

Its intensity will depend on the grain size. The peak intensity increases rapidly with increasing grain size [29, 30]. The electron-phonon coupling in microparticles is weakened with decrease in size due to the decrease in the density of states for both the electrons and the phonons [31]. The peak at 218 cm^{-1} is sharp and intense, which indicates the high structural crystallinity of the microparticles synthesized on stainless steel. In the spectrum, a less intense peak is observed at 296 cm^{-1} which is attributed to the A_g mode of the CuO phase. The only allowed Raman phonon mode of Cu_2O is observed at 515 cm^{-1} which is also known as the active Raman T_{2g} mode of Cu_2O, the Raman active modes of Cu_2O are due to the relative motion of oxygen atoms and the band at 638 cm^{-1} is attributed to the TO phonon mode.

3.1. SEM analysis

The morphology of the Cu_2O microparticles were analysed by SEM as shown in Fig. 4; a) shows the agglomerations of the Cu_2O microparticles grown on the stainless steel surface at 10 μm, of which small randomly scattered dots are observed on the deposited surface. A more definite form of the Cu_2O microparticles, presenting a spherical morphology, can be observed in Fig. 4b). The agglomerations observed by the micro-graphs can cause the formation of long islands which can be generated thanks to the formation of the microparticles in spherical form on the surface of the stainless steel which the distance of separation varies one with respect to the other as can be seen in 4c), which can cause the analyzed surface to look like an island.

The possible mechanism of formation of microparticles can be explained as follows: first, Cu^{2+} reacts with enough OH- species which comes from the dissociation of CH_3CH_2OH [27, 32]. In the synthesis process, the formation of the copper species reduces the concentration of free Cu^{2+} ions in the plasma mixture, which promotes slow growth of Cu_2O particles. A slow formation rate leads to separation of the nucleation and growth process, which is important for high-quality crystal synthesis. Then, at an elevated temperature inside the reaction chamber, it allows the complex to react with the OH- generated in the plasma to form Cu_2O nuclei. In the next step, the small Cu_2O particles aggregate

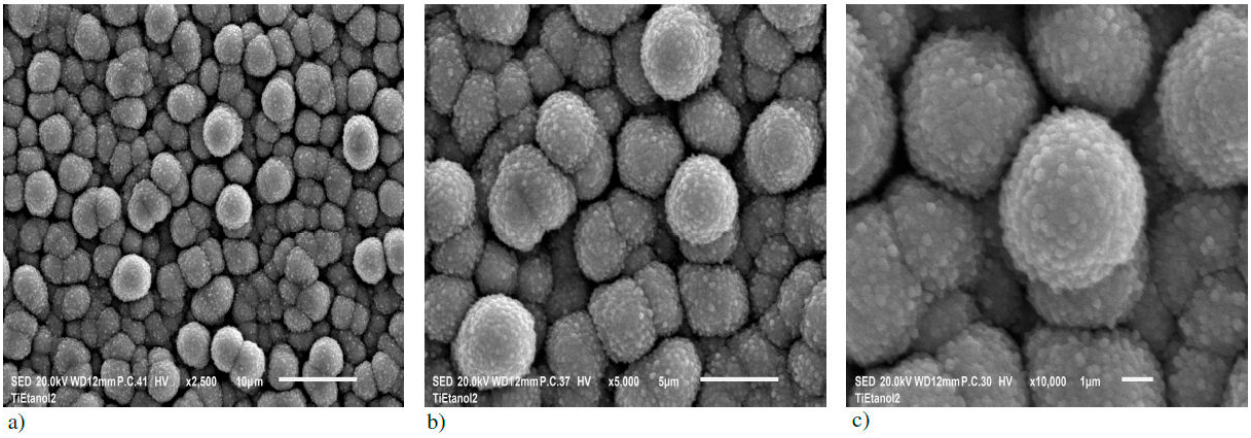

FIGURE 4. SEM micrographs of the microparticles spherical produced by CH_3CH_2OH-N_2 plasma, a) 10, b) 5 and c) 1μm.

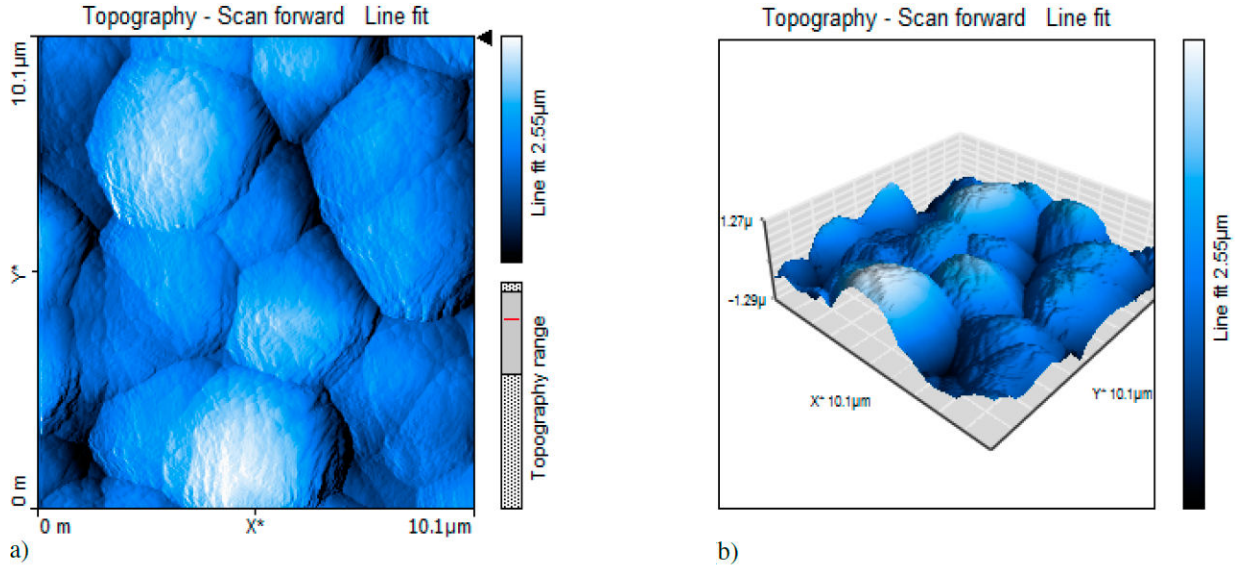

FIGURE 5. 2-D a) and 3-D b) images of the microparticles of Cu_2O obtained by AFM.

to form microparticles and due to the minimal energy needed to form spherical geometries these grow into spherical Cu_2O microparticles, which has demonstrated by means of Raman spectroscopy that there is a presence of crystalline phases within the analysed samples [32].

3.2. AFM analysis

Figure 5 presents the images obtained by AFM on the stainless steel surface showing the morphology of the Cu_2O microparticles. In Fig. 5 aggregates of spherical particles can be observed, from where it is possible to see the formation of planes and valleys as can be seen in the 3-D images. The roughness of the film samples of the present study are analysed by using Scanning Probe Image Processor (SPIP) software. The value obtained for the roughness according to the results obtained by SPIP was 20 nm and a grain size of 48 nm, from which for frequencies around 30 kHz a more homogeneous distribution of spherical microparticles on the surface can be expected of stainless steel [34]. That is why in the 3-D images it is possible to appreciate that the difference between the peaks and valleys caused by the distribution of the microparticles and the non-orientation of these is minimal one with respect to the other. Studies have shown that for frequencies greater than 80 kHz the difference is notable between valleys and peaks, which causes a significant increase in roughness [34, 35]. The 2-D images demonstrate the formation of the microparticles in spherical form with a non-homogeneous distribution and the separation distance varies one with respect to the other as a consequence of their agglomeration and their non-orientation.

3.3. EDS analysis

Figure 6 shows stoichiometry of the film obtained thanks to the microparticles of Cu_2O. The samples were analyzed by EDS in different areas to corroborate only the existence of atoms of Cu, O and stainless steel (iron, zinc, chromium and sulphur).

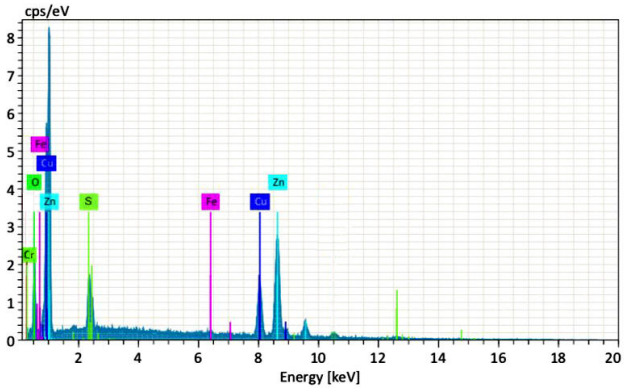

FIGURE 6. EDS spectra of the Cu_2O thin films with atomic ratio of 2:1.

TABLE II. Percentage of atoms in the analysed sample.

Element	**Atom [%]** 10 μm	**Atom [%]** 5 μm	**Atom [%]** 1 μm
Cooper	38.10	39.21	41.01
Oxygen	17.24	19.45	19.30
Zinc	41.30	38.49	36.13
Iron	0.51	0.58	1.01
Chromium	2.10	2.03	2.14
Sulphur	0.76	0.24	0.41

Table II shows the percentage of species present within the analysed sample. The EDS spectra (Fig. 6) clearly demonstrate the presence of only peaks corresponding to Cu, O and the stainless steel elements (Zn, Fe, Cr, S). The observed atomic ratio is 2:1, as can be seen in Table II between the elements Cu and O, which corroborates the presence of the Cu_2O phase owing to the CH_3CH_2OH-N_2 plasma mixture.

4. Conclusions

In summary, spherical Cu_2O microparticles were successfully grown on a stainless steel substrate using a Cu blank, by PVD technique in its pulsed Sputtering form, with a $CH3CH_2OH$-N_2 mixture. The dissociation of CH_3CH_2OH within the discharge is taken advantage of, because when the molecule dissociates we can find the formation of OH radicals, the OH bonds within the plasma can be broken to take advantage of the O atoms, which can interact with the surface of the target, which are capable of expelling the Cu atoms that, when interacting with the O atoms, can react and form the Cu_2O phase deposited on the surface of stainless steel in the form of spheres. The results show that the Cu_2O oxidized phase can be produced and it has been confirmed by Raman and EDS analysis, of which is obtained an atomic ratio of 2:1 between the elements Cu and O, which corroborates the presence of Cu_2O. The SEM and AFM results show the morphology of the grown structures which can be observed that for each case they present a spherical shape, the SEM analyzes show agglomerations of spherical microparticles while the AFM results again show the spherical morphology of the microparticles, where the formation of valleys and peaks can be seen. The roughness value and the grain size is determined by SPIP which gives the results of 20 nm for the roughness and a grain size of 45 nm, therefore the implementation of the plasma mixture of CH_3CH_2OH-N_2 can be an option to be able to generate Cu_2O microparticles.

Acknowledgments

The authors thank the projects DGAPA [IN-02916], CONACyT [268644], PROMEP [103.5/13/6626], PRODEP [DSA/103.5/15/6986], PII-43/PIDE/2013, UAEMex 4307/2017/CI and [CA-5511-6/18-8304].

1. M. Heinemann, B. Eifert, and C. Heiliger, Band structure and phase stability of the copper oxides Cu_2O, CuO and Cu_4O_3. *Phys. Rev. B*, **87** (2013) 115111, https://doi.org/10.1103/PhysRevB.87.115111
2. A. S. Zoolfakar, R. A. Rani, A. J. Morfa, A. P. O'Mullane, and K. Kalantarzadeh, Nanostructured copper oxide semiconductors: A perspective on materials, synthesis methods and applications. *J. Mater. Chem. C*, **2** (2014) 5247, https://doi.org/10.1039/C4TC00345D
3. K. P. Mulsselman, A. Marin, L. Schmidt-Mende, and J. L. Macmanus-Driscoll, Incompatible lenght scales in nanostructured Cu_2O solar cell. *Adv. Funct. Mater.* **22** (2012) 2202, https://doi.org/10.1002/ADFM.201102263
4. P. K. Pagare and A. P. Torane, Band gap varied cuprous oxide (Cu_2O) thin films as a tool for glucose sensing. *Microchim Acta* **183** (2016) 2983, https://doi.org/10.1007/s00604-016-1949-6
5. Y. Kwon, A. Soon, and H. Han Hand Lee, Shape effects of cuprous oxide particles on stability in wáter and photocatalytic wáter splitting. *J. Mater. Chem. A.* **3** (2015) 156, https://doi.org/10.1039/C4TA04863F
6. L. Brisse, P. Stevens, G. Toussaint, O. Crosnier and T. Brousse, Performance and limitations of Cu_2O:Graphene composite electrode materials for aqueous hybrid electrochemical capacitors. *Electrochim Acta* **279** (2018) 161, https://doi.org/10.1016/j.electacta.2018.04.202
7. G.-Z. Yuan, C.-F. Hsia, Z.-W. Lin, C. Chiang, Y.-W. Chiang, and M. H. Huang, *Chem. Eur. J.* **22** (2016) 12548, https://doi.org/10.31349/RevMexFis.64.326
8. W. Wang, Z. Liu, Y. Liu, C. Xu, C. Zheng and G. Wang, A simple wet chemical synthesis and characterization of CuO nanorods. *Appl. Phys. A*, **76** (2003) 417, https://doi.org/10.1007/s00339-002-1514-5

9. T. Chtouki, S. Taboukhat, H. Kavak, A. Zawadzka, and H. Erguig, Elidrissi Band Sahraoui B, Characterization and third harmonic generation calculations of undoped and doped spin-coated multilayered CuO thin films. *J. Phys. Chem. Solids* **124** (2019) 60, https://doi.org/10.1016/j.jpcs.2018.08.035

10. A. S. Zoolfakar, R. A. Rani, A. J. Morfa, S., A. P. O'Mullane, and K. Kalantar-Zadeh, Nanostructured copper oxide semiconductors: a perspective on materials, synthesis methods and applications. *J. Mater. Chem. C.* **22** (2014) 5247, https://doi.org/10.1039/C4TC00345D

11. Y. Alajiani *et al.*, Characterisation of Cu_2O, Cu_4O_3, and CuO mixed phase thin films produced by microwave-activated reactive sputtering. *Vacuum,* **144** (2017) 217, https://doi.org/10.1016/j.vacuum.2017.08.005

12. B. Zhou *et al.*, Enhanced photocatalytic activity of flowerlike Cu_2O/Cu prepared using solvent-thermal route. *Mater. Chem. Phys.* **126** (2011) 847, https://doi.org/10.1016/j.matchemphys.2010.12.030

13. M. H. Huang, and P. H. Lin, Shape-Controlled Synthesis of Polyhedral Nanocrystals and Their Facet-Dependent Properties. *Adv. Funct. Mater.* **22** (2012) 14, https://doi.org/10.1002/adfm.201101784

14. Y. Xu, H. Wang, Y. Yu, L. Tian, W. Zhao, and B. Zhang, Cu_2O Nanocrystals: Surfactant-Free Room-Temperature Morphology-Modulated Synthesis and Shape-Dependent Heterogeneous Organic Catalytic Activities, *J. Phys. Chem. C.* **115** (2011) 15288, https://doi.org/110.1021/jp204982q

15. Y. Gu, X. Ye, Y. Zhang, and C. Wang, Template-free Fabrication of Nano-sized Cu_2O Hollow Spheres, Sheets and Octahedrons in Cu-citrate System and their Morphology-dependent Semiconductor Type. *Curr. Nanosci.* **8** (2012) 417, https://doi.org/10.2174/157341312800620296

16. X. L. Luo, Y. F. Han, D. S. Yang, and Y. S. Chen, Solvo-Thermal Synthesis of Cu_2O Micro-Spheres and Their Catalytic Performance for Thermal Decomposition of Ammonium Perchlorate. *Acta Phys. Chim. Sin.* **28** (2012) 297, https://doi.org/10.3866/PKU.WHXB201112012

17. W. Chen, L. Li, Q. Peng, and Y. Li, Polyol synthesis and chemical conversion of Cu_2O nanospheres. *Nano Res.* **5** (2012) 320, https://doi.org/10.1007/s12274-012-0212-7

18. W. Huang, L. Lyu, Y. Yang, and M. H. Huang, Synthesis of Cu_2O Nanocrystals from Cubic to Rhombic Dodecahedral Structures and Their Comparative Photocatalytic Activity. *J. Am. Chem. Soc.* **134** (2011) 1261, https://doi.org/10.1021/ja209662v

19. S. K. Li *et al.*, Rapid synthesis of flower-like Cu_2O architectures in ionic liquids by the assistance of microwave irradiation with high photochemical activity. *Dalton Trans.* **40** (2011) 6745, https://doi.org/10.1039/C0DT01794A

20. G. Borcia, C. A. Anderson, and N. M. D. Brown, Dielectric barrier discharge for surface treatment: application to selected polymers in film and fibre form. *Plasma Sources Sci. Technol.* **12** (2003) 335, https://doi.org/10.1088/0963-0252/12/3/306

21. G. Borcia, C. A. Anderson, and N. M. D. Brown, The surface oxidation of selected polymers using an atmospheric pressure air dielectric barrier discharge. Part I. *Appl Surf Sci.* **221** (2004) 203, https://doi.org/10.1016/S0169-4332(03)00879-1

22. R. Morent, Comparison between XPS- and FTIR-analysis of plasma-treated polypropylene film surfaces. *Surf Interface Anal* **40** (2008) 597, https://doi.org/10.1002/sia.2619

23. N. De Geyter, R. Morent, and C. Leys, Surface characterization of plasma-modified polyethylene by contact angle experiments and ATR-FTIR spectroscopy. *Surf Interface Anal* **40** (2008) 608, https://doi.org/10.1002/sia.2611

24. S. Guimond *et al*., Biaxially Oriented Polypropylene (BOPP) Surface Modification by Nitrogen Atmospheric Pressure Glow Discharge (APGD) and by Air Corona. *Plasmas and Polym.* **7** (2002) 71, https://doi.org/10.1023/A:1015274118642

25. R. Maurau *et al*., Nitrogen Introduction in pp-HMDSO Thin Films Deposited by Atmospheric Pressure Dielectric Barrier Discharge: An XPS Study. *Plasma Processes Polym.* **9** (2012) 316, https://doi.org/10.1002/ppap.201100144

26. P. G. Reyes, A. Gómez, H. Martíez, O. Flores, C. Torres, and J. Vergara, Characterization of Ethanol Plasma Glow Discharge, Decomposition in Several Species and Solid Film Formation. *IEEE Transactions on Plasma Science* **44** (2016) 2995, https://doi.org/10.1109/TPS.2016.2628639

27. S. Perusquía *et al*., Experimental Study of Ethanol and Helium Mixture Glow Discharge. *IEEE Transactions on Plasma Science* **47** (2019) 445, https://doi.org/10.1109/TPS.2018.2863716

28. A. Van Deynse, C. Leys, R. Morent, and N. De Geyter, Plasma Polymerization in a Nitrogen/Ethanol Dielectric Barrier Discharge: A Parameter Study. *Plasma Chemistry and Plasma Processing* **39** (2019) 1317, https://doi.org/10.1007/s11090-019-10007-8

29. S. B. Schmitt-Rink, D. A. Miller, and D. S. Chemla, Theory of the linear and nonlinear optical properties of semiconductor microcrystallites. *Phys. Rev. B.* **35** (1987) 8113, https://doi.org/10.1103/PhysRevB.35.8113.

30. M. C. Klein, F. Hache, D. Ricard, and C. Flytzanis, Size dependence of electron-phonon coupling in semiconductor nanospheres: The case of CdSe. *Phys. Rev. B.* **42** (1990) 11123, https://doi.org/10.1103/PhysRevB.42.11123

31. M. Cardona, Light Scattering in Solids. *Springer, Berlin, (1983)*. https://doi.org/10.1007/978-3-642-84206-1_10.

32. L. C. Chen, Review of preparation and optoelectronic characteristics of Cu_2O-based solar cells with nanostructure, *Materials Science in Semiconductor Processing*, **16** (2013) 1172, https://doi.org/10.1016/j.mssp.2012.12.028

33. Y. Nishi *et al.*, Influence of Cu_2O surface treatment on the photovoltaic properties of Al-doped ZnO/Cu_2O solar cells. *Thin Solid Films* **520** (2012) 3819, https://doi.org/10.1016/j.tsf.2011.08.032

34. D.-H. Kim *et al.*, Structure and electrical transport properties of bismuth thin films prepared by RF magnetron sputtering. *Applied Surface Science* **252** (2006) 3525, https://doi.org/10.1016/j.apsusc.2005.05.046

35. S. Mammeri *et al.*, Sputtering and surface state evolution of Bi under oblique incidence of 120 keV Ar^+ ions. *Nuclear Instruments and Methods in Physics Research Section B: Beam Interactions with Materials and Atoms* **269** (2011) 909, https://doi.org/10.1016/j.nimb.2010.12.003